Supplementary Information (SI) for Nanoscale.
This journal is © The Royal Society of Chemistry 2026

Electrocatalytic Activity Enhancement on Nitrobenzene Reduction via the *p–d* Orbital Hybridization from Single- to Dual-Atom Catalysis

Mingqiang Liu [a], Yi Yang [a], Xiaoqing Gong [a], Yuanyuan Yu [a], Xiaohong Song [a], Kefeng Xie [a, *]

[a]School of Chemistry and Chemical Engineering, Lanzhou Jiaotong University, Lanzhou, 730070, China.

* Correspondence: xiekefeng@mail.lzjtu.cn.

Table S1. The four reaction paths of NBRR and the elementary reactions corresponding to each reaction path (*: Active site).

Pathway	Elementary reaction
Pathway 1	$PhNO_2 \rightarrow *PhNO_2 \rightarrow *PhNOOH \rightarrow *PhNO \rightarrow *PhNOH \rightarrow *PhN \rightarrow *PhNH \rightarrow *PhNH_2 \rightarrow PhNH_2$
	$PhNO_2 + * \rightarrow *PhNO_2$
	$*PhNO_2 + *H + e^- \rightarrow *PhNOOH$
	$*PhNOOH + *H + e^- \rightarrow *PhNO + H_2O$
	$*PhNO + *H + e^- \rightarrow *PhNOH$
	$*PhNOH + *H + e^- \rightarrow *PhN + H_2O$
	$*PhN + *H + e^- \rightarrow *PhNH$
	$*PhNH + *H + e^- \rightarrow *PhNH_2$
	$*PhNH_2 \rightarrow PhNH_2 + *$
Pathway 2	$PhNO_2 \rightarrow *PhNO_2 \rightarrow *PhNOOH \rightarrow *PhNO \rightarrow *PhNOH \rightarrow *PhNHOH \rightarrow *PhNH \rightarrow *PhNH_2 \rightarrow PhNH_2$
	$PhNO_2 + * \rightarrow *PhNO_2$

	$*PhNO_2 + *H + e^- \rightarrow *PhNOOH$
	$*PhNOOH + *H + e^- \rightarrow *PhNO + H_2O$
	$*PhNO + *H + e^- \rightarrow *PhNOH$
	$*PhNOH + *H + e^- \rightarrow *PhNHOH$
	$*PhNHOH + *H + e^- \rightarrow *PhNH + H_2O$
	$*PhNH+ *H + e^- \rightarrow *PhNH_2$
	$*PhNH_2 \rightarrow PhNH_2 + *$
Pathway 3	$PhNO_2 \rightarrow *PhNO_2 \rightarrow *PhNOOH \rightarrow *PhN(OH)_2 \rightarrow *PhNOH \rightarrow *PhNHOH \rightarrow *PhNH \rightarrow *PhNH_2 \rightarrow PhNH_2$
	$PhNO_2 + * \rightarrow *PhNO_2$
	$*PhNO_2 + *H + e^- \rightarrow *PhNOOH$
	$*PhNOOH + *H + e^- \rightarrow *PhN(OH)_2$
	$*PhN(OH)_2 + *H + e^- \rightarrow *PhNOH + H_2O$
	$*PhNOH + *H + e^- \rightarrow *PhNHOH$
	$*PhNHOH + *H + e^- \rightarrow *PhNH + H_2O$
	$*PhNH+ *H + e^- \rightarrow *PhNH_2$
	$*PhNH_2 \rightarrow PhNH_2 + *$
Pathway 4	$PhNO_2 \rightarrow *PhNO_2 \rightarrow *PhNOOH \rightarrow *PhN(OH)_2 \rightarrow *PhNOH \rightarrow *PhN \rightarrow *PhNH \rightarrow *PhNH_2 \rightarrow PhNH_2$
	$PhNO_2 + * \rightarrow *PhNO_2$
	$*PhNO_2 + *H + e^- \rightarrow *PhNOOH$
	$*PhNOOH + *H + e^- \rightarrow *PhN(OH)_2$
	$*PhN(OH)_2 + *H + e^- \rightarrow *PhNOH + H_2O$
	$*PhNOH + *H + e^- \rightarrow *PhN + H_2O$
	$*PhN + *H + e^- \rightarrow *PhNH$
	$*PhNH+ *H + e^- \rightarrow *PhNH_2$
	$*PhNH_2 \rightarrow PhNH_2 + *$

Table S2. The lattice parameters of optimized crystal structures of 14 TMN_4-G

monolayers.

MN_4-G	Crystal structure	Lattice constant
CoN_4-G	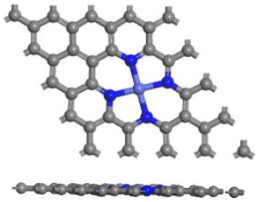	a= 9.84 b= 9.84 c= 20.00
CuN_4-G	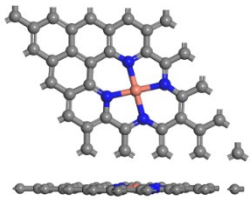	a= 9.80 b= 9.80 c= 19.93
NiN_4-G	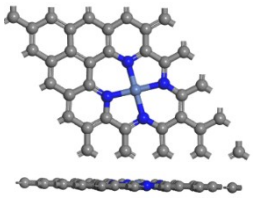	a= 9.84 b= 9.84 c= 20.00
FeN_4-G	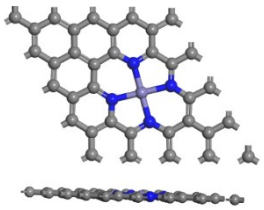	a= 9.85 b= 9.85 c= 20.03
PdN_4-G	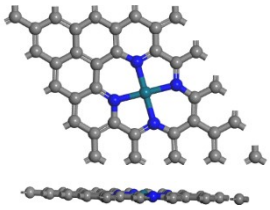	a= 9.94 b= 9.94 c= 20.20
AuN_4-G	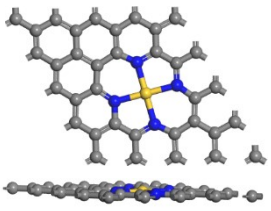	a= 9.85 b= 9.85 c= 20.21

AgN_4-G	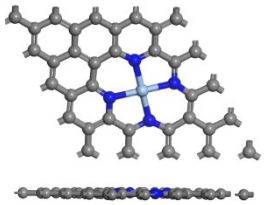	a= 9.98 b= 9.98 c=20.28
CdN_4-G	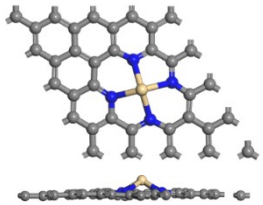	a= 9.97 b= 9.97 c=20.26
IrN_4-G	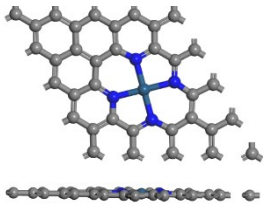	a= 9.93 b= 9.93 c= 20.19
MoN_4-G	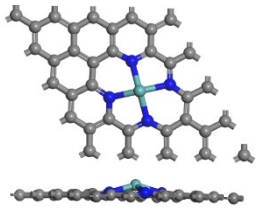	a= 9.93 b= 9.93 c= 20.19
RhN_4-G	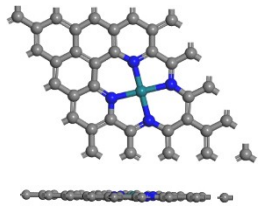	a= 9.93 b= 9.93 c= 20.18
MnN_4-G	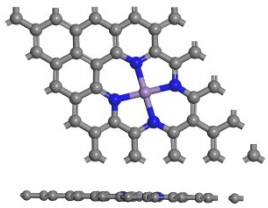	a= 9.88 b= 9.88 c= 20.07
ZnN_4-G	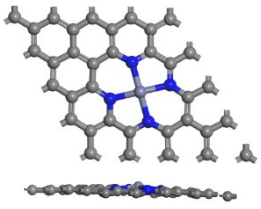	a= 9.76 b= 9.76 c= 19.84

CrN_4-G	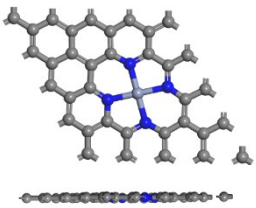	a= 9.90 b= 9.90 c= 20.12

Table S3. The d_{M-N}, d_{N-O1}, d_{N-O2}, d_{M-O1}, and E_{ads} (side on), E_{ads} (end on) of 10 SACs.

TM	d_{M-N} (Å)	d_{N-O1} (Å)	d_{N-O2} (Å)	d_{M-O1} (Å)	E_{ads}(side on)	E_{ads}(end on)
$PhNO_2$	/	1.237	1.237	/	/	/
Co	1.89	1.266	1.241	2.51	-0.94	-0.34
Cu	1.92	1.246	1.240	2.85	-1.08	-0.84
Ni	1.89	1.243	1.24	2.83	-0.95	-0.26
Fe	1.90	1.274	1.241	2.25	-1.08	-0.27
Pd	1.98	1.243	1.240	2.81	-0.94	-0.20
Ir	1.97	1.241	1.239	3.01	-0.95	-0.41
Mo	2.05	1.378	1.248	1.96	-1.82	-1.23
Rh	1.97	1.258	1.254	2.37	-0.93	-0.74
Mn	1.93	1.285	1.243	2.23	-1.23	-0.84
Cr	1.96	1.317	1.247	2.04	-1.52	-0.78
Au	2.01	/	/	/	/	/
Ag	2.03	/	/	/	/	/
Cd	2.21	/	/	/	/	/
Zn	1.94	/	/	/	/	/

Table S4. E_b, E_f and U_{diss} of TMN_4-G,and the adsorption energy of $PhNO_2$ on the catalyst.

TM	E_b	E_f	Ne	U_{diss}^{0} (V)	U_{diss}	rate-determining step
Co	-7.80	-3.87	2	-0.28	1.66	$*PhNO_2 \rightarrow *PhNOOH$
Cu	-5.74	-1.82	2	0.34	1.25	$*PhNO_2 \rightarrow *PhNOOH$
Ni	-7.66	-3.74	2	-0.26	1.61	$*PhNO_2 \rightarrow *PhNOOH$
Fe	-7.14	-3.22	2	-0.45	1.16	$*PhNO_2 \rightarrow *PhNOOH$
Pd	-5.54	-1.62	2	0.95	1.76	$*PhNO_2 \rightarrow *PhNOOH$
Ir	-7.79	-3.86	1	1.16	5.02	$*PhNO_2 \rightarrow *PhNOOH$
Mo	-7.79	-3.87	3	-0.2	1.09	$*PhNH \rightarrow *PhNH_2$
Rh	-6.98	-3.06	2	0.6	2.13	$*PhNO_2 \rightarrow *PhNOOH$
Mn	-6.65	-2.73	2	-1.19	0.18	$*PhNO_2 \rightarrow *PhNOOH$
Cr	-7.67	-3.75	2	-0.91	0.97	$*PhNO_2 \rightarrow *PhNOOH$
Au	-2.53	1.40	3	1.5	1.03	/
Ag	-2.22	1.70	1	0.8	-0.90	/
Cd	-1.54	2.38	2	-0.4	-1.59	/
Zn	-3.79	0.13	2	-0.76	-0.82	/

Table S5. Free energy for the intermediates.

Intermediates	*$PhNO_2$	*PhNOOH	*PhNO	*PhNOH	*PhN	*PhNH	*$PhNH_2$	*$PhN(OH)_2$	*PhNHOH
Co	-1.04	-0.78	-2.25	-2.29	-2.91	-4.20	-5.02	-0.74	-2.85
Cu	-1.22	-0.58	-1.96	-1.88	-2.25	-3.71	-4.96	-0.80	-2.76
Ni	-1.07	-0.57	-1.80	-1.97	-2.07	-3.57	-4.86	-0.71	-2.66
Fe	-1.19	-0.91	-2.59	-2.50	-3.31	-4.40	-5.07	-0.72	-2.83
Pd	-1.07	-0.49	-1.76	-1.84	-1.88	-3.31	-4.87	-0.70	-2.67
Ir	-1.11	-0.67	-2.36	-2.51	-3.17	-4.33	-5.00	-0.65	-2.85
Mo	-1.99	-3.14	-5.07	-4.49	-6.76	-6.56	-5.75	-4.68	-3.75
Rh	-1.01	-0.72	-2.19	-2.45	-3.01	-4.30	-4.85	-0.72	-2.64
Mn	-1.31	-0.73	-2.42	-2.53	-3.63	-4.55	-5.15	-1.06	-2.98
Cr	-1.60	-1.29	-2.87	-3.04	-4.37	-5.06	-5.22	-1.15	-3.01

Table S6. U_L, ΔG_{max} of 10 catalysts and ΔG of HER.

catalysts	U_L	ΔG_{max}	ΔG(HER)
Co	-0.26	0.26	0.38
Cu	-0.64	0.64	1.67
Ni	-0.5	0.5	1.42
Fe	-0.28	0.28	0.43
Pd	-0.58	0.58	1.52
Ir	-0.45	0.45	-0.46
Mo	-0.81	0.81	-0.42
Rh	-0.29	0.29	-0.24
Mn	-0.58	0.58	0.56
Cr	-0.31	0.31	0.46

Table S7. $h_{M1\text{-}M2}$, $d_{M1\text{-}M2}$, and corresponding lattice parameters of 10 DACs.

catalysts	$h_{Co\text{-}M}$ (Å)	$d_{Co\text{-}M}$ (Å)	$d_{Co\text{-}N1}$ (Å)	$d_{Co\text{-}N2}$ (Å)	$d_{Co\text{-}N3}$ (Å)	$d_{M\text{-}N1}$ (Å)	$d_{M\text{-}N2}$ (Å)	$d_{M\text{-}N3}$ (Å)	a (Å)	b (Å)	c (Å)
Co-Al	0.00	2.35	1.88	1.98	1.94	1.93	1.93	1.96	14.80	14.80	20.06
Co-Ga	0.05	2.65	1.94	2.00	1.91	2.15	2.17	2.45	14.70	14.70	19.92
Co-Ge	0.05	2.52	1.92	2.00	1.91	2.09	2.13	2.35	14.71	14.71	19.93
Co-In	0.09	2.80	1.99	1.99	1.91	2.51	2.55	2.73	14.86	14.86	20.13
Co-Sn	0.07	2.74	1.96	1.97	1.91	2.31	2.38	2.43	14.80	14.80	20.06
Co-Sb	0.06	2.56	1.91	1.95	1.92	2.27	2.36	2.27	14.81	14.81	20.07
Co-Tl	0.10	2.81	1.98	1.90	1.83	2.60	2.70	2.73	14.77	14.77	20.01
Co-Pb	0.08	2.79	1.96	1.96	1.90	2.43	2.54	2.53	14.80	14.80	20.06
Co-Bi	0.07	2.53	1.92	1.95	1.91	2.35	2.40	2.36	14.81	14.81	20.07
Co-Co	0.00	2.34	1.93	1.96	1.87	1.87	1.96	1.93	14.77	14.77	20.00

Table S8. E_{ABE}, E_{ACOH}, E_{ABE}-E_{ACOH}, E_{form}, U_{diss} of 10 DACs.

Catalysts	E_{ABE}	E_{ACOH}	E_{ABE} - E_{ACOH}	E_{form} (eV)	Ne	U_{diss}^{0} (V)	U_{diss}
Co-Al	-7.46	-5.05	-2.41	-4.62	3	-0.24	1.61
Co-Ga	-6.59	-3.90	-2.70	-3.75	3	0.32	1.81
Co-Ge	-6.11	-4.55	-1.55	-3.26	2	0.71	2.34
Co-In	-7.08	-4.13	-2.95	-4.23	3	0.42	2.11
Co-Sn	-7.19	-4.44	-2.75	-4.34	2	0.52	2.69
Co-Sb	-5.25	-4.35	-0.90	-2.40	3	0.71	1.67
Co-Tl	-6.88	-3.93	-2.95	-4.03	2	-0.23	1.79
Co-Pb	-7.12	-4.35	-2.77	-4.27	2	0.69	2.83
Co-Bi	-5.88	-4.37	-1.51	-3.03	1	0.84	2.86
Co-Co	-6.32	-5.62	-0.70	-3.47	2	1.18	2.92

Table S9. The change of N-O bond and the adsorption energy of parallel adsorption and vertical adsorption when $PhNO_2$ is adsorbed on DACs.

/	$d_{N\text{-}O1}$	$d_{N\text{-}O2}$	E_{ads} (side on)	E_{ads} (end on)
NB	1.237	1.237	/	/
Co-Al	1.382	1.297	-1.88	-1.50
Co-Ga	1.349	1.325	-1.05	-0.94
Co-Ge	1.273	1.246	-1.09	-0.67
Co-In	1.276	1.314	-1.28	-1.05
Co-Sn	1.259	1.272	-1.32	-1.23
Co-Sb	1.268	1.275	-1.08	-0.77
Co-Tl	1.274	1.319	-1.27	-0.96
Co-Pb	1.259	1.256	-1.23	-1.00
Co-Bi	1.288	1.272	-1.01	-0.84
Co-Co	1.291	1.286	-1.44	-1.11

Table S10. The Gibbs free energy ΔG_{max}(NBRR), U_L (NBRR) of 10 DACs NBRR PDS and the Gibbs free energy ΔG(HER) and U_L (HER) of hydrogen evolution reaction.

	ΔG_{max} (NBRR)	ΔG (HER)	U_L (NBRR)	U_L (HER)
Co-Al	0.57	-0.55	-0.57	0.55
Co-Ga	0.48	-0.05	-0.48	0.05
Co-Ge	0.3	0.44	-0.3	-0.44
Co-In	0.21	0.37	-0.21	-0.37
Co-Sn	0.32	0.38	-0.32	-0.38
Co-Sb	0.3	0.35	-0.3	-0.35
Co-Tl	0.26	0.34	-0.26	-0.34
Co-Pb	0.44	0.35	-0.44	-0.35
Co-Bi	0.18	0.38	-0.18	-0.38
Co-Co	0.46	-0.28	-0.46	0.28

Table S11. Four reaction pathways for the reduction of $-NO_2$ in *p*-$ClC_6H_4NO_2$ over Co-Bi-N_6V_4-G DAC and the elementary reactions corresponding to each reaction pathway were proposed (*: Active site).

Pathway	Elementary reaction
Pathway 1	$ClC_6H_4NO_2 \rightarrow ClC_6H_4NO_2^* \rightarrow ClC_6H_4NOOH^* \rightarrow ClC_6H_4NO^* \rightarrow ClC_6H_4NOH^* \rightarrow ClC_6H_4N^* \rightarrow ClC_6H_4NH^* \rightarrow ClC_6H_4NH_2^* \rightarrow ClC_6H_4NH_2$
	$ClC_6H_4NO_2 + * \rightarrow *ClC_6H_4NO_2$
	$*ClC_6H_4NO_2 + *H + e^- \rightarrow *ClC_6H_4NOOH$
	$*ClC_6H_4NOOH + *H + e^- \rightarrow *ClC_6H_4NO + H_2O$
	$*ClC_6H_4NO + *H + e^- \rightarrow *ClC_6H_4NOH$
	$*ClC_6H_4NOH + *H + e^- \rightarrow *ClC_6H_4N + H_2O$
	$*ClC_6H_4N + *H + e^- \rightarrow *ClC_6H_4NH$
	$*ClC_6H_4NH+ *H + e^- \rightarrow *ClC_6H_4NH_2$
	$*ClC_6H_4NH_2 \rightarrow ClC_6H_4NH_2 + *$
Pathway 2	$ClC_6H_4NO_2 \rightarrow *ClC_6H_4NO_2 \rightarrow *ClC_6H_4NOOH \rightarrow *ClC_6H_4NO \rightarrow *ClC_6H_4NOH \rightarrow *ClC_6H_4NHOH \rightarrow *ClC_6H_4NH \rightarrow *ClC_6H_4NH_2 \rightarrow ClC_6H_4NH_2$
	$*ClC_6H_4NO_2 + * \rightarrow *ClC_6H_4NO_2$
	$*ClC_6H_4NO_2 + *H + e^- \rightarrow *ClC_6H_4NOOH$
	$*ClC_6H_4NOOH + *H + e^- \rightarrow *ClC_6H_4NO + H_2O$
	$*ClC_6H_4NO + *H + e^- \rightarrow *ClC_6H_4NOH$
	$*ClC_6H_4NOH + *H + e^- \rightarrow *ClC_6H_4NHOH$
	$*ClC_6H_4NHOH + *H + e^- \rightarrow *ClC_6H_4NH + H_2O$
	$*ClC_6H_4NH+ *H + e^- \rightarrow *ClC_6H_4NH_2$
	$*ClC_6H_4NH_2 \rightarrow ClC_6H_4NH_2 + *$
Pathway 3	$ClC_6H_4NO_2 \rightarrow *ClC_6H_4NO_2 \rightarrow *ClC_6H_4NOOH \rightarrow *ClC_6H_4N(OH)_2 \rightarrow *ClC_6H_4NOH \rightarrow *ClC_6H_4NHOH \rightarrow *ClC_6H_4NH \rightarrow *ClC_6H_4NH_2 \rightarrow ClC_6H_4NH_2$
	$ClC_6H_4NO_2 + * \rightarrow *ClC_6H_4NO_2$
	$*ClC_6H_4NO_2 + *H + e^- \rightarrow *ClC_6H_4NOOH$
	$*ClC_6H_4NOOH + *H + e^- \rightarrow *ClC_6H_4N(OH)_2$

	$*ClC_6H_4N(OH)_2 + *H + e^- \rightarrow *ClC_6H_4NOH + H_2O$
	$*ClC_6H_4NOH + *H + e^- \rightarrow *ClC_6H_4NHOH$
	$*ClC_6H_4NHOH + *H + e^- \rightarrow *ClC_6H_4NH + H_2O$
	$*ClC_6H_4NH+ *H + e^- \rightarrow *ClC_6H_4NH_2$
	$*ClC_6H_4NH_2 \rightarrow ClC_6H_4NH_2 + *$
Pathway 4	$ClC_6H_4NO_2 \rightarrow *ClC_6H_4NO_2 \rightarrow *ClC_6H_4NOOH \rightarrow *ClC_6H_4N(OH)_2 \rightarrow$ $*ClC_6H_4NOH \rightarrow *ClC_6H_4N \rightarrow *ClC_6H_4NH \rightarrow *ClC_6H_4NH_2 \rightarrow ClC_6H_4NH_2$
	$ClC_6H_4NO_2 + * \rightarrow *ClC_6H_4NO_2$
	$*ClC_6H_4NO_2 + *H + e^- \rightarrow *ClC_6H_4NOOH$
	$*ClC_6H_4NOOH + *H + e^- \rightarrow *ClC_6H_4N(OH)_2$
	$*ClC_6H_4N(OH)_2 + *H + e^- \rightarrow *ClC_6H_4NOH + H_2O$
	$*ClC_6H_4NOH + *H + e^- \rightarrow *ClC_6H_4N + H_2O$
	$*ClC_6H_4N + *H + e^- \rightarrow *ClC_6H_4NH$
	$*ClC_6H_4NH+ *H + e^- \rightarrow *ClC_6H_4NH_2$
	$*ClC_6H_4NH_2 \rightarrow ClC_6H_4NH_2 + *$

Table S12. The reaction pathway of −Cl reduction in *p*-$ClC_6H_4NO_2$ over Co-Bi-N_6V_4-G DAC and the corresponding elementary reactions (*: Active site).

Pathway	Elementary reaction
Pathway	$ClC_6H_4NO_2 \rightarrow *ClC_6H_4NO_2 \rightarrow *HClC_6H_4NO_2 \rightarrow *C_6H_4NO_2$
	$\rightarrow *C_6H_5NO_2 \rightarrow C_6H_5NO_2$
	$ClC_6H_4NO_2 + * \rightarrow *ClC_6H_4NO_2$
	$*ClC_6H_4NO_2 + *H + e^- \rightarrow *HClC_6H_4NO_2$
	$*HClC_6H_4NO_2 \rightarrow *C_6H_4NO_2 + HCl$
	$*C_6H_4NO_2 + *H + e^- \rightarrow *C_6H_5NO_2$
	$*C_6H_5NO_2 \rightarrow C_6H_5NO_2 + *$

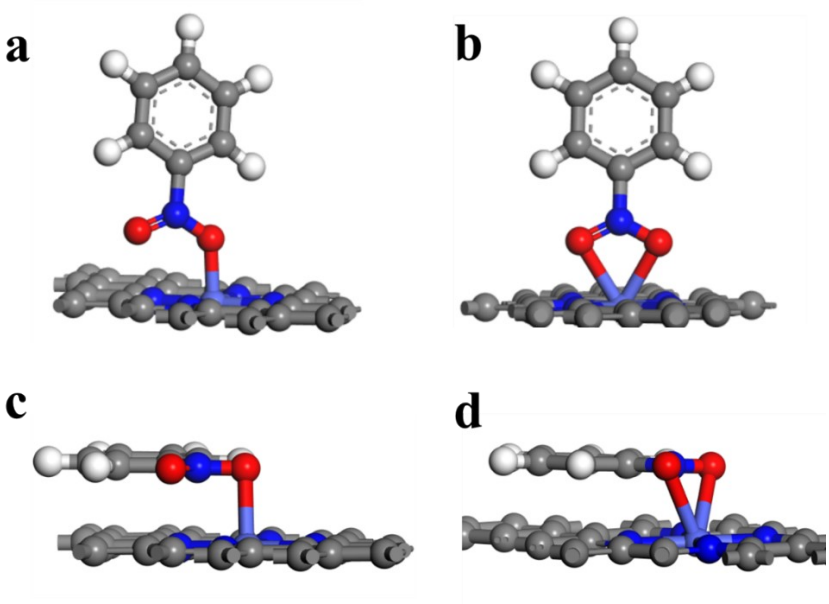

Fig. S1 (a) Vertical monodentate adsorption of $PhNO_2$ on TM-N_4-G. (b) Vertical bidentate adsorption of $PhNO_2$ on TM-N_4-G. (c) Parallel monodentate adsorption of $PhNO_2$ on TM-N_4-G. (d) Parallel bidentate adsorption of $PhNO_2$ on TM-N_4-G.

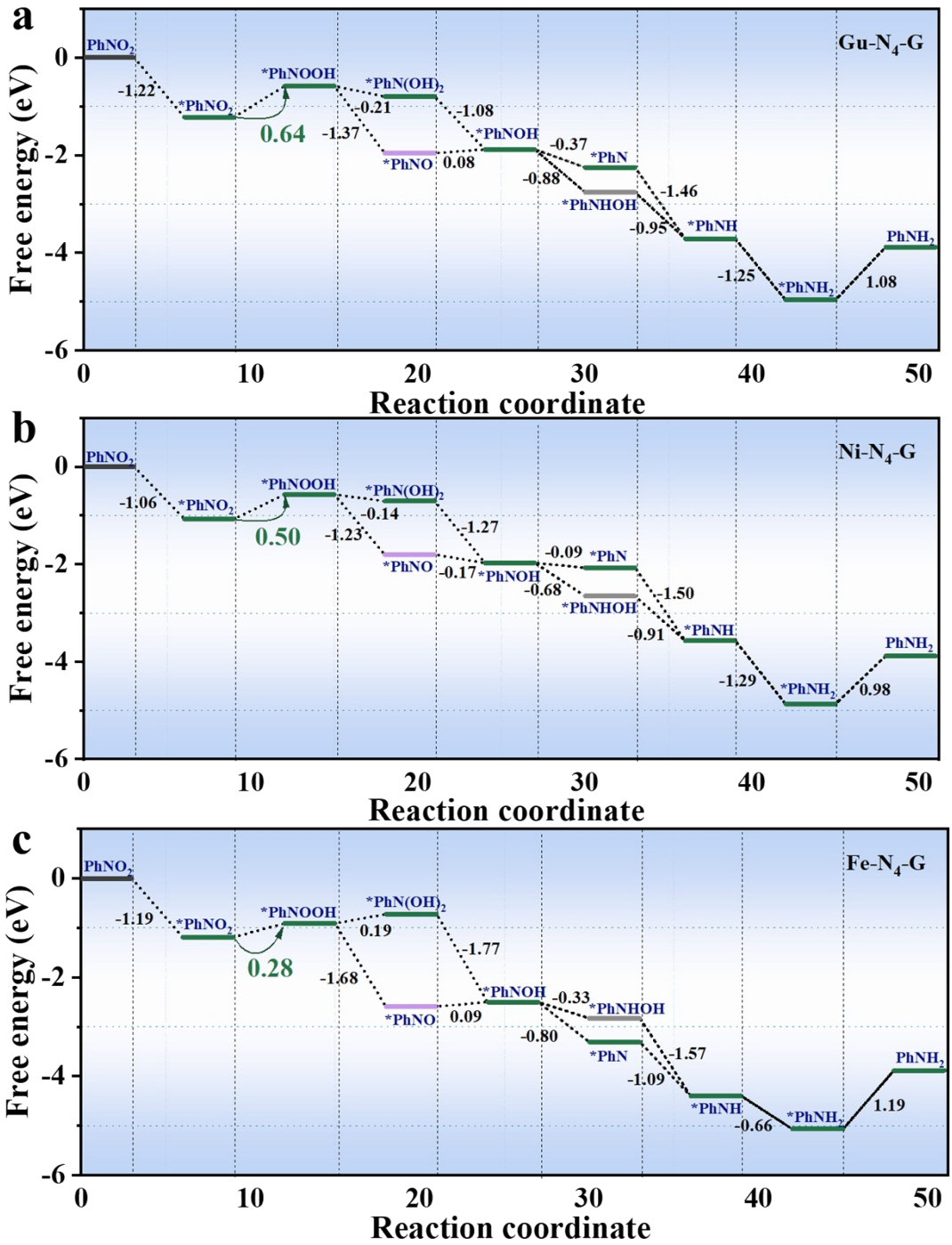

Fig. S2 The free energy diagrams of four reaction paths of Cu-N_4-G, Ni-N_4-G, Fe-N_4-G SAC were obtained.

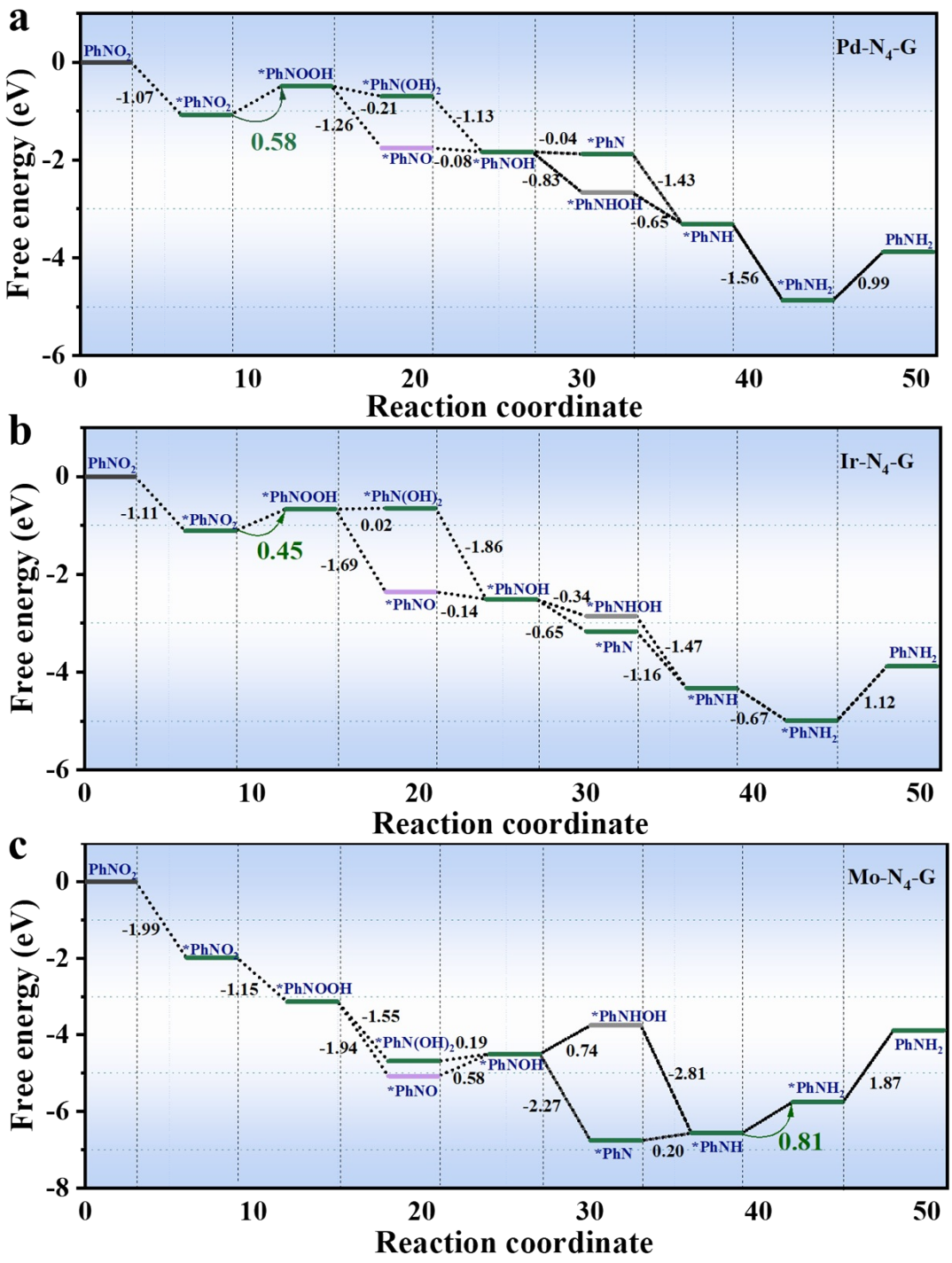

Fig. S3 The free energy diagrams of the four reaction paths of Pd-N_4-G, Ir-N_4-G, Mo-N_4-G SAC were plotted.

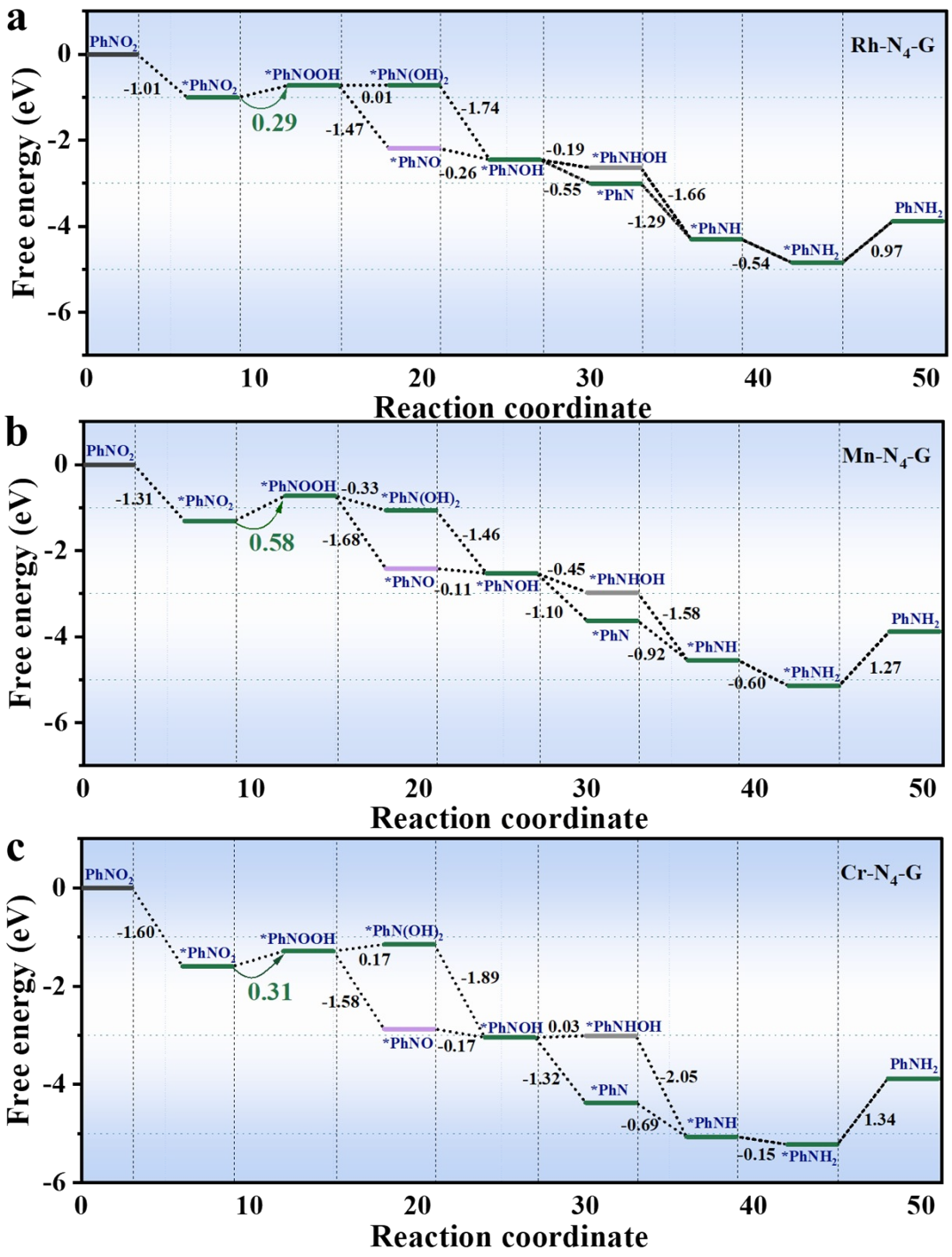

Fig. S4 The free energy diagrams of four reaction paths of Rh-N_4-G, Mn-N_4-G, Cr-N_4-G SAC were obtained.

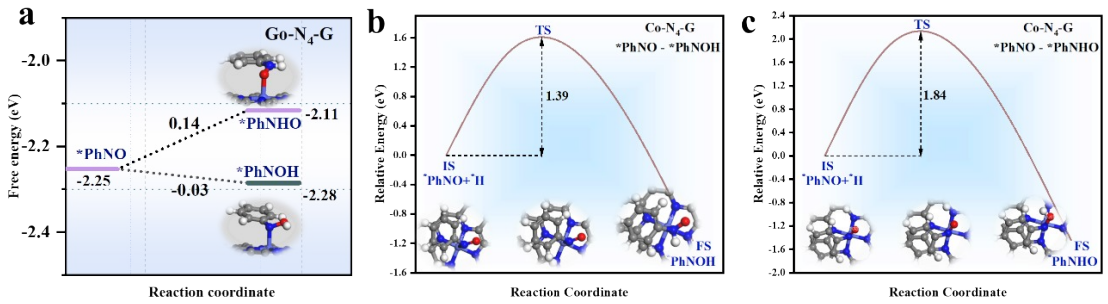

Fig. S5

(a) The free energy diagrams of *PhNO → *PhNOH and *PhNO → *PhNHO elementary reactions.

(b-c) Kinetic analysis of *PhNO → *PhNOH and *PhNO → *PhNHO elementary reactions.

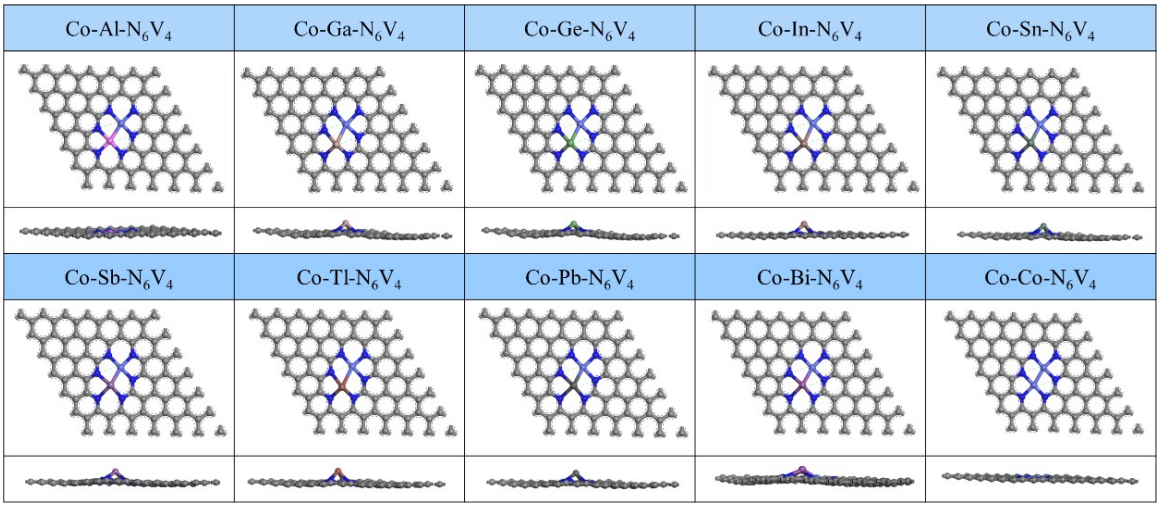

Fig. S6 The structure diagram of the optimized Co-M-N_6V_4 DACs.

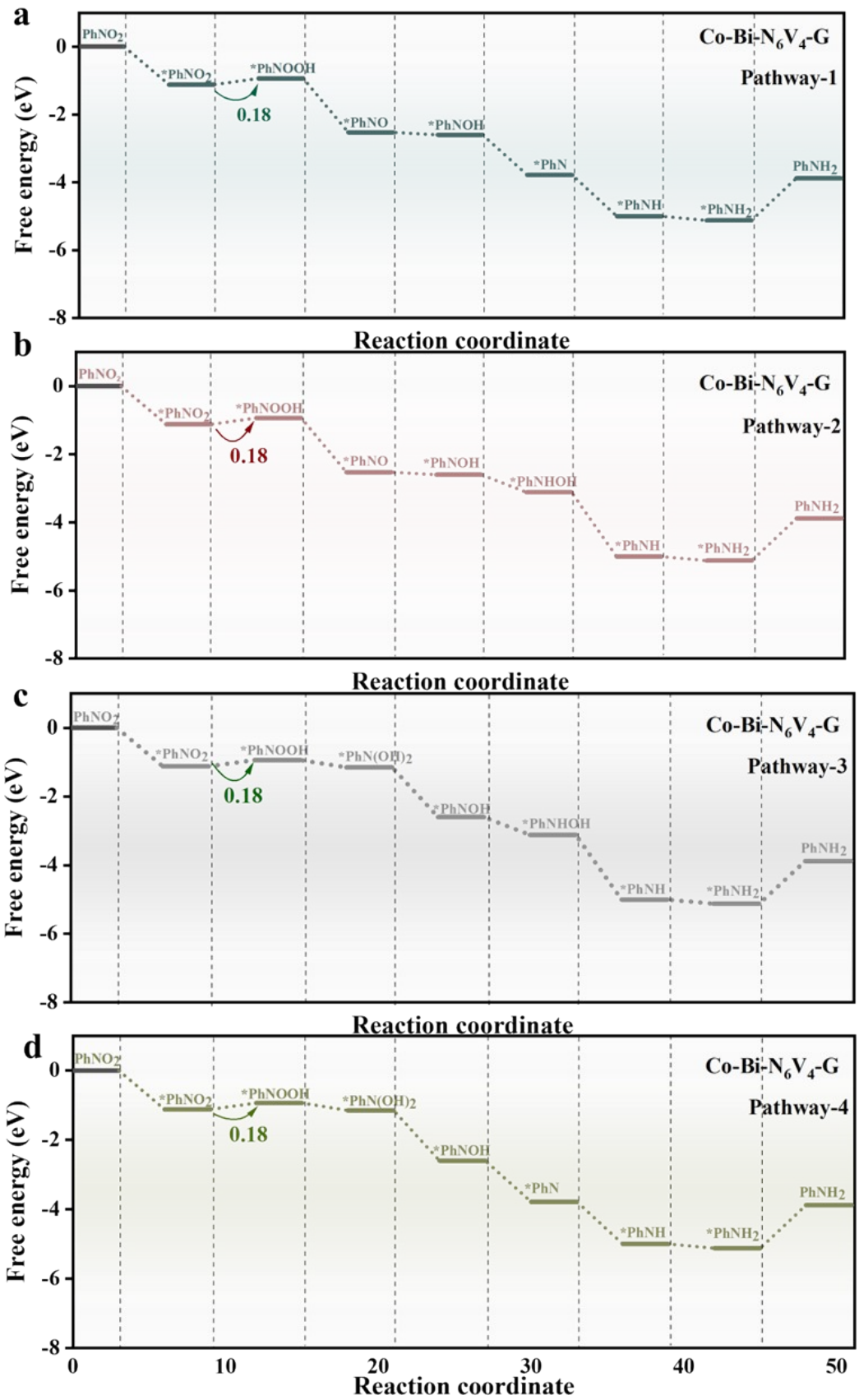

Fig. S7 (a-b) The free energy diagrams of four reaction paths of Co-Bi-N_6V_4-G DAC.

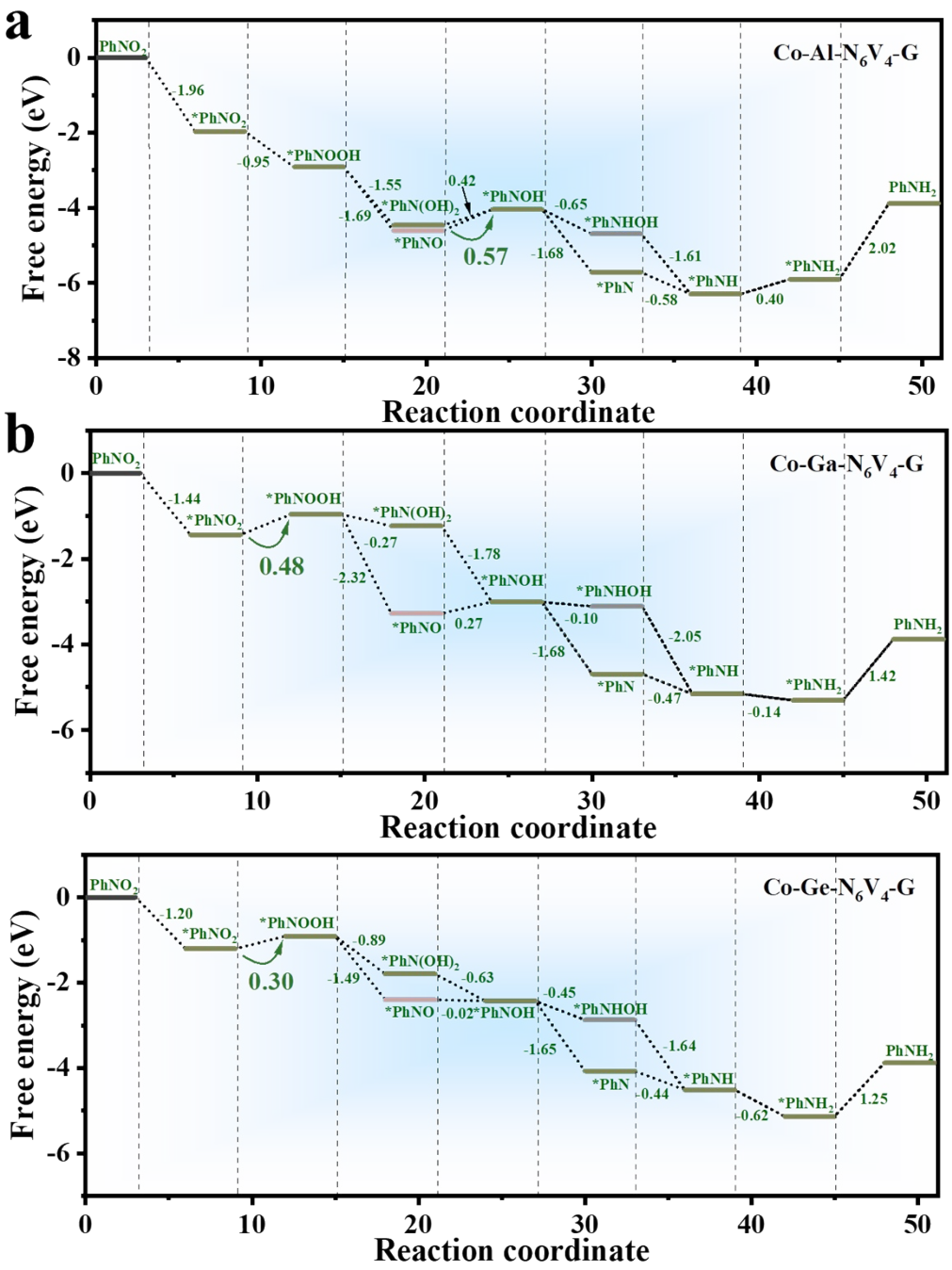

Fig. S8 The total free energy diagrams of Co-Al-N_6V_4-G, Co-Ga-N_6V_4-G and Co-Ge-N_6V_4-G DACs.

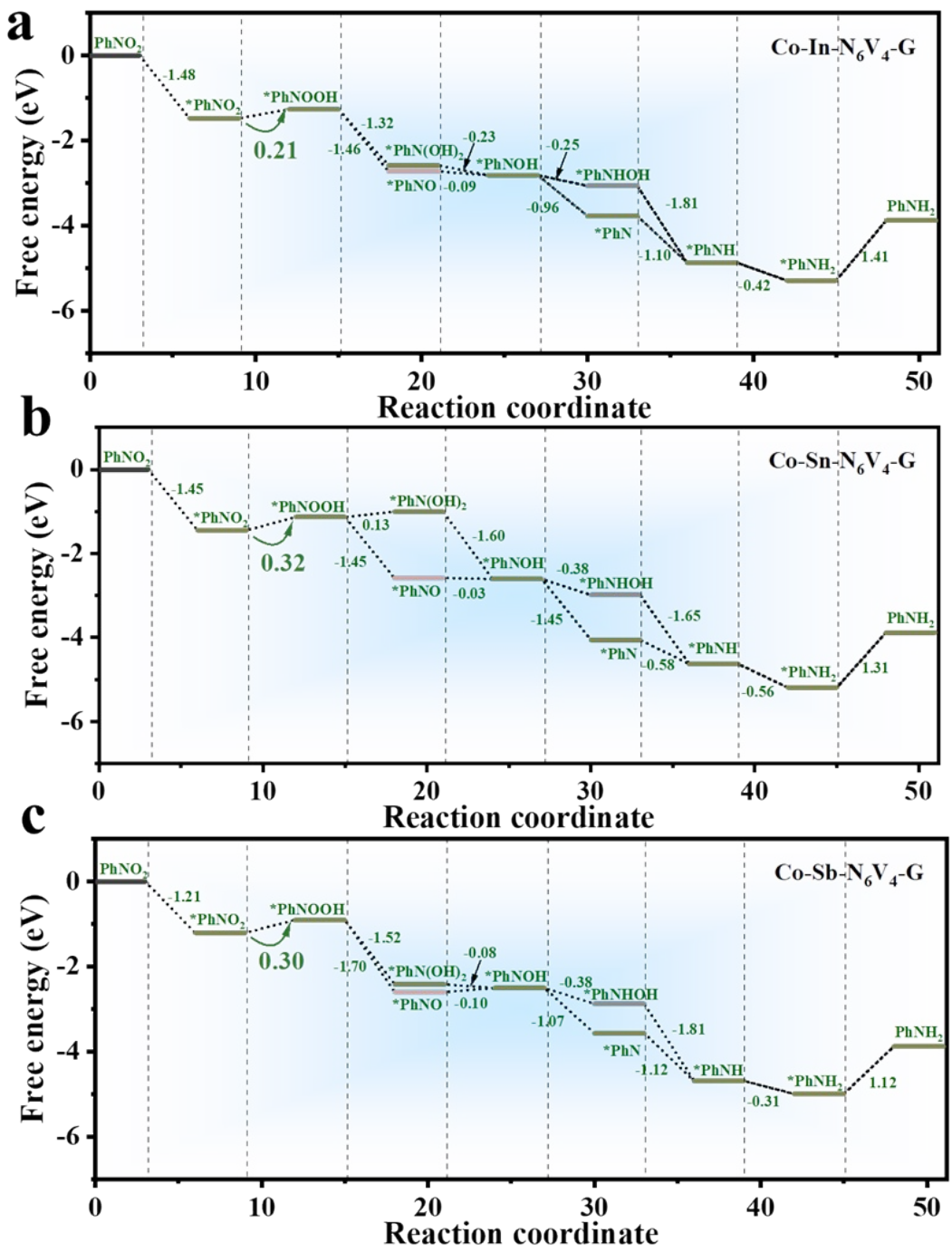

Fig. S9 The total free energy diagrams of Co-In-N_6V_4-G, Co-Sn-N_6V_4-G and Co-Sb-N_6V_4-G DACs.

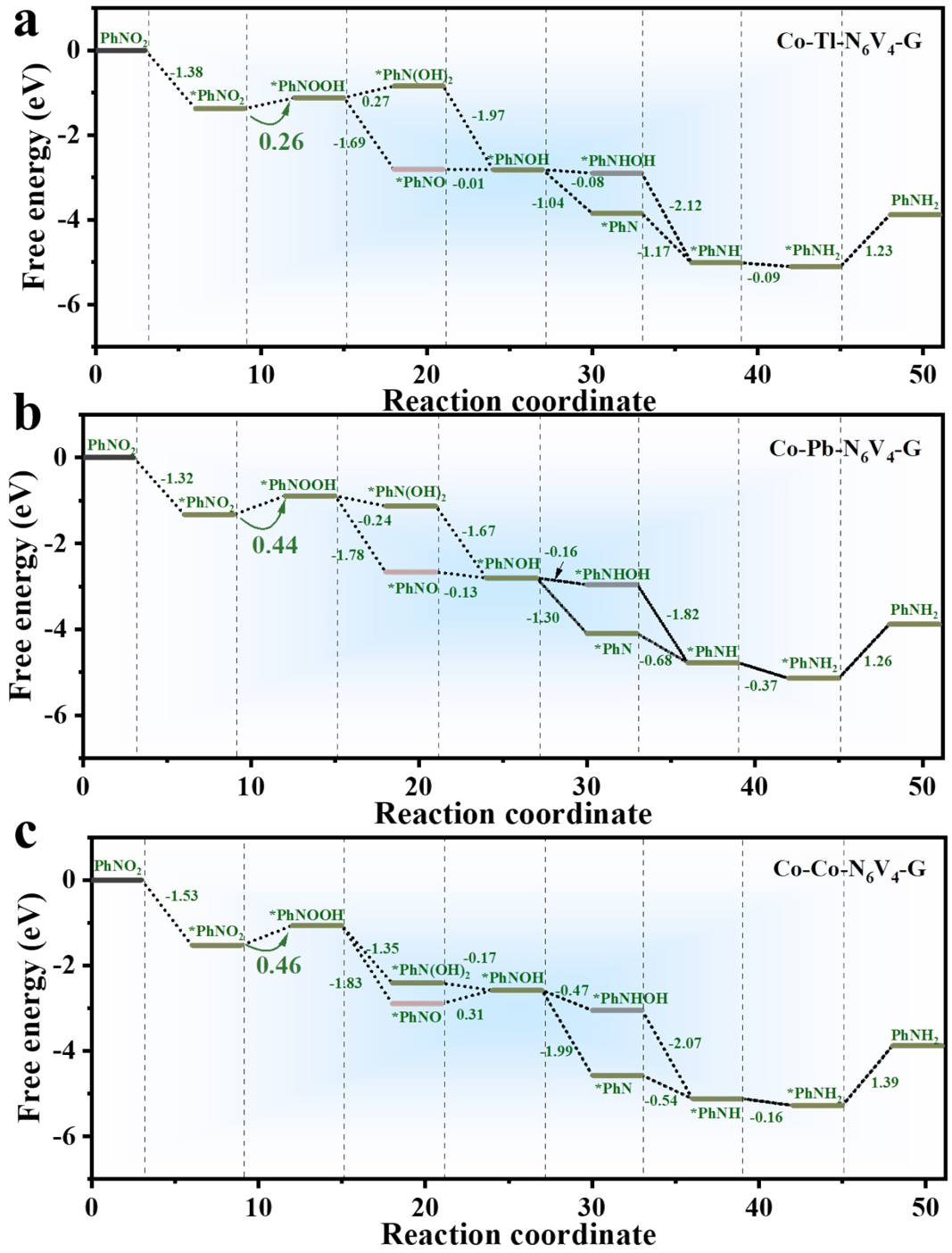

Fig. S10 The total free energy diagrams of Co-Tl-N_6V_4-G, Co-Pb-N_6V_4-G and Co-Co-N_6V_4-G DACs.

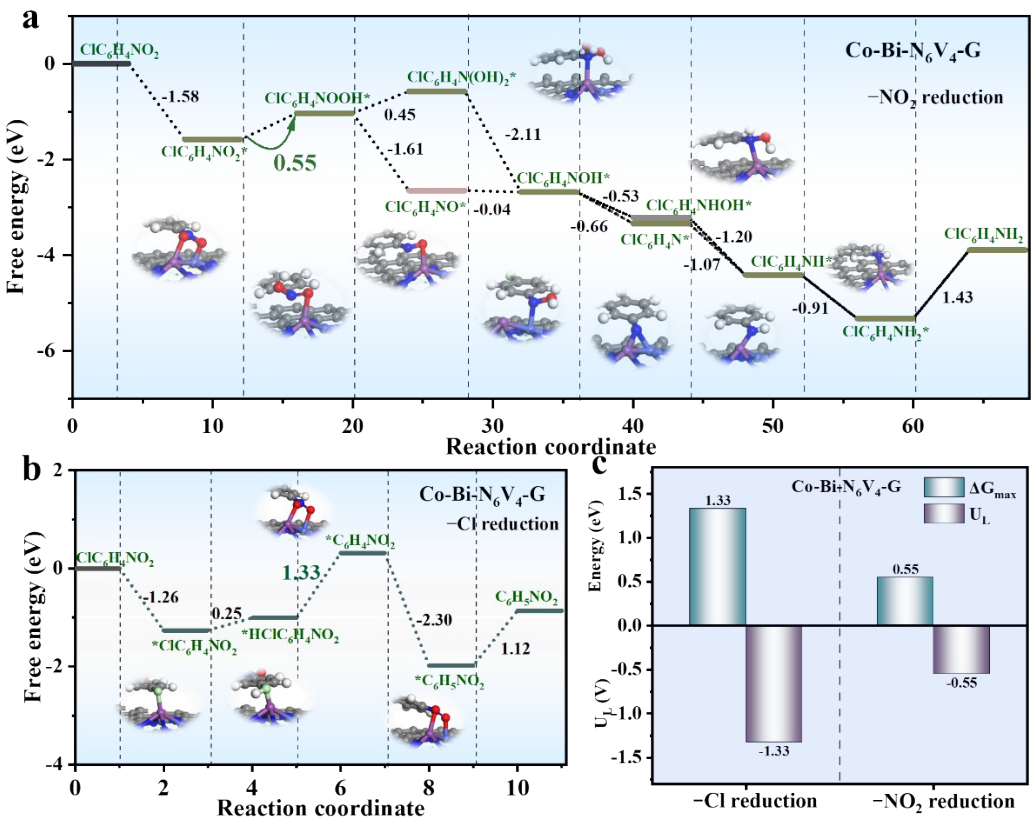

Fig.S11 (a) The free energy diagram of the $-NO_2$ reduction pathway in *p*-$ClC_6H_4NO_2$ and the optimal intermediate configuration on Co-Bi-N_6V_4-G DAC. (b) The free energy diagram of the −Cl reduction pathway in *p*-$ClC_6H_4NO_2$ and the optimal intermediate configuration on Co-Bi-N_6V_4-G DAC. (c) ΔG_{max} and U_L of the $-NO_2$ reduction pathway and the −Cl reduction pathway.

Halogenated anilines and their derivatives, as key organic intermediates in the large-scale production of drugs and fine chemicals, are usually prepared via the reduction reaction of the corresponding halogenated nitrobenzene [1]. Designing catalysts that can inhibit the hydrogenolysis of carbon–halogen bonds to improve selectivity is the core challenge of this type of reaction. Therefore, herein, *p*-$ClC_6H_4NO_2$ was used as the catalytic substrate, and the Co-Bi-N_6V_4-G DAC was selected as the representative catalyst. By calculating different reaction paths, the selective reduction mechanism on the Co-Bi-N_6V_4-G DAC was explored. The reduction path of $-NO_2$ in *p*-$ClC_6H_4NO_2$ is similar to that of $PhNO_2$, which involves six PCET steps. The total reaction is as follows: *p*-$ClC_6H_4NO_2$ + $6H^+$ +$6e^-$ → *p*-$ClC_6H_4NH_2$ + $2H_2O$. The reduction path of −Cl contains two PCET steps, and the total

reaction is as follows: *p*-$ClC_6H_4NO_2$ + $2H^+$ +$2e^-$ → $C_6H_5NO_2$ + HCl (Table S11, Table S12). The path for the reduction of −NO_2 in *p*-$ClC_6H_4NO_2$ on the Co-Bi-N_6V_4-G DAC and the optimal intermediate configuration are shown in Fig. S11a. The results show that the optimal reaction path is Pathway 1. The specific process is as follows: *p*-$ClC_6H_4NO_2$ → *p*-$ClC_6H_4NO_2$* → *p*-ClC_6H_4NOOH* → *p*-ClC_6H_4NO* → *p*-ClC_6H_4NOH* → *p*-ClC_6H_4N* → *p*-ClC_6H_4NH* →*p*-$ClC_6H_4NH_2$* → *p*-$ClC_6H_4NH_2$, where the PDS is *p*-$ClC_6H_4NO_2$* → *p*-ClC_6H_4NOOH*. The path for the reduction of −Cl in *p*-$ClC_6H_4NO_2$ on the Co-Bi-N_6V_4-G DAC and the optimal intermediate configuration are shown in Fig. S11b, where the PDS is *$HClC_6H_4NO_2$ → *$C_6H_4NO_2$. Further comparisons show that the ΔG_{max} of the −NO_2 and −Cl reduction paths are 0.55 eV and 1.33 eV, respectively, and the corresponding U_L are − 0.55 V and − 1.33 V, respectively (Fig. S11c). These results show that the −NO_2 of *p*-$ClC_6H_4NO_2$ can be preferentially reduced on the Co-Bi-N_6V_4-G DAC. Hence, the Co-Bi-N_6V_4-G DAC exhibits excellent catalytic activity and selectivity for the reduction of *p*-$ClC_6H_4NO_2$.

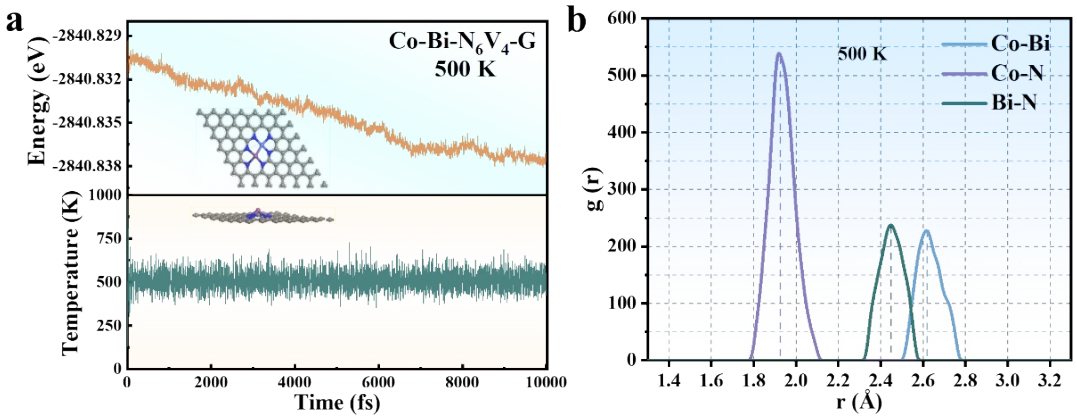

Fig. S12 AIMD and radial distribution function of Co-Bi-N_6V_4-G DAC at 500 K.

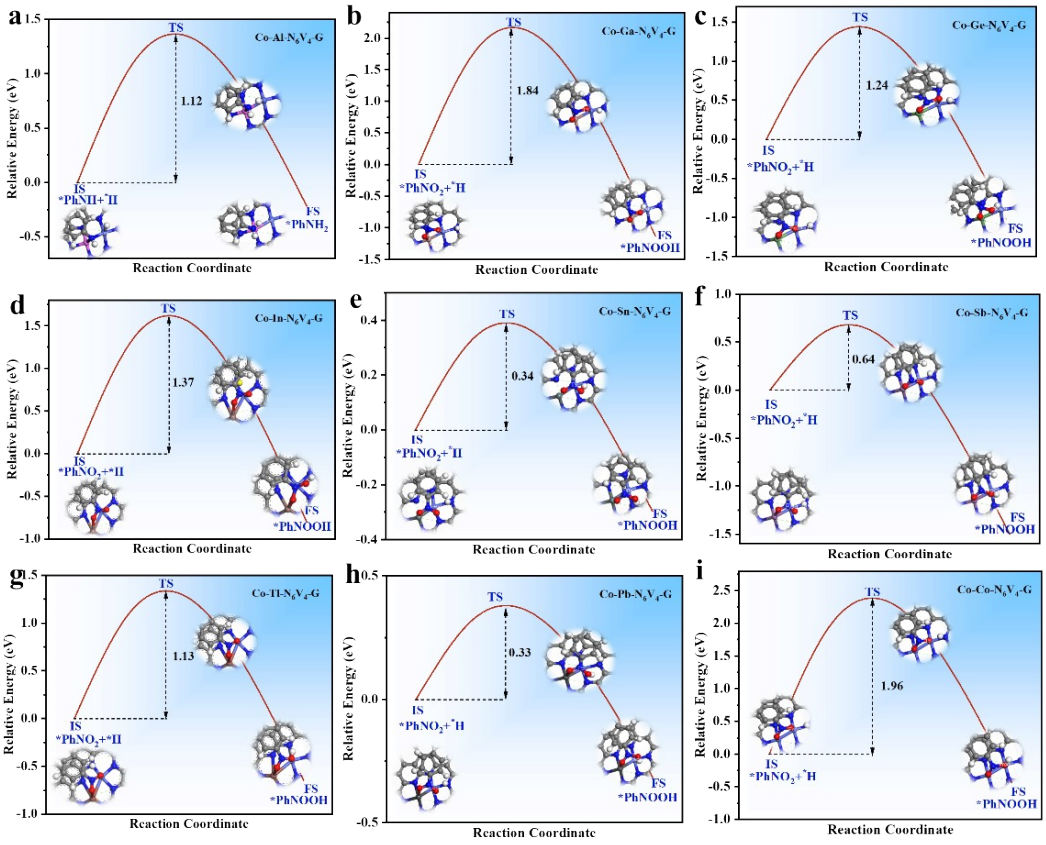

Fig. S13 (a-i) Co-Al-N_6V_4-G, Co-Ga-N_6V_4-G, Co-Ge-N_6V_4-G, Co-In-N_6V_4-G, Co-Sn-N_6V_4-G, Co-Sb-N_6V_4-G, Co-Tl-N_6V_4-G, Co-Pb-N_6V_4-G, Co-Co-N_6V_4-G catalysts for PDS reaction energy barrier.

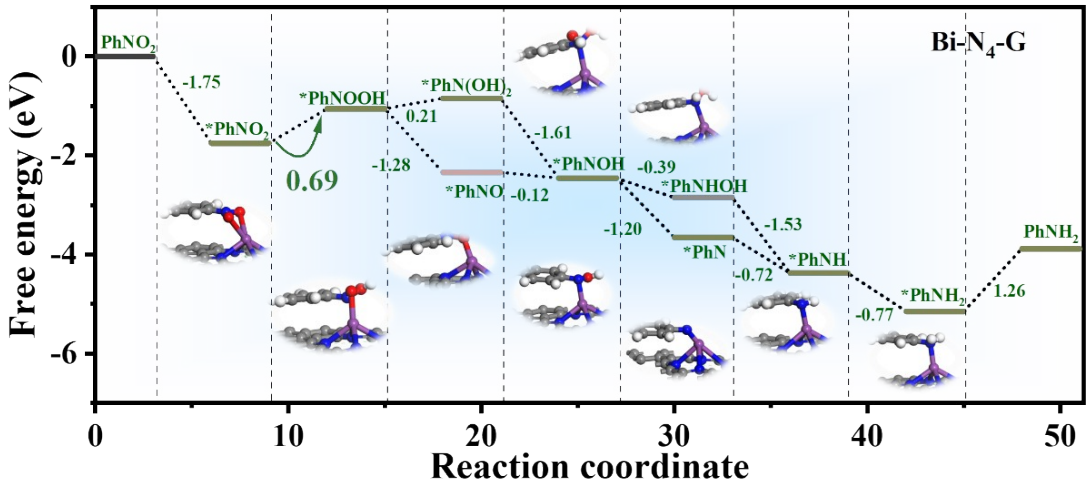

Fig. S14 Total path free energy diagram of NBRR on Bi-N_4-G.

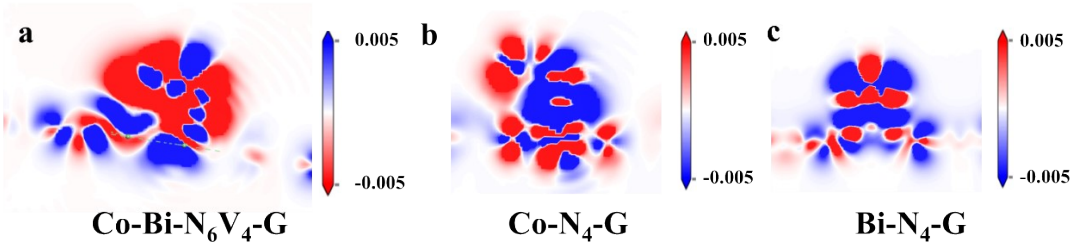

Fig. S15 (a-c) Two-dimensional slice images of Co-Bi-N_6V_4-G DAC, Bi-N_4-G and Co-N_4-G SAC CDD.

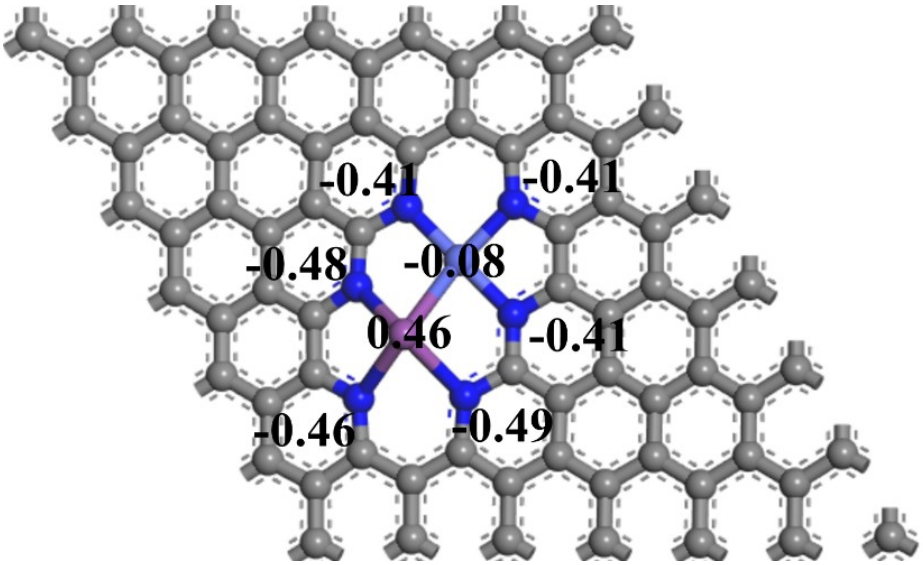

Fig. S16 The Mulliken charge transfer of Co-Bi-N_6V_4-G DAC.

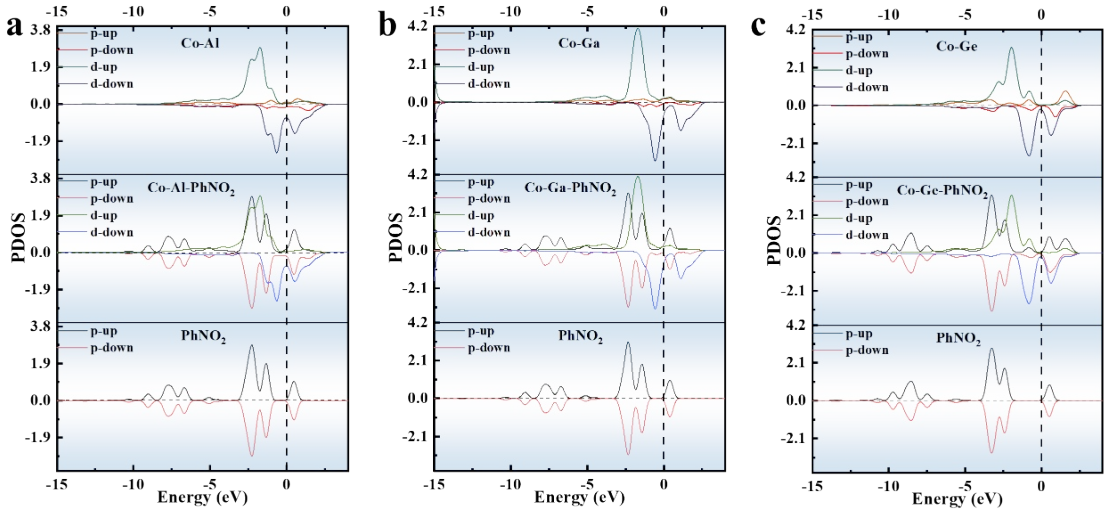

Fig. S17 The PDOS of $PhNO_2$ adsorbed on Co-Al-N_6V_4-G, Co-Ga-N_6V_4-G, Co-Ge-N_6V_4-G DACs.

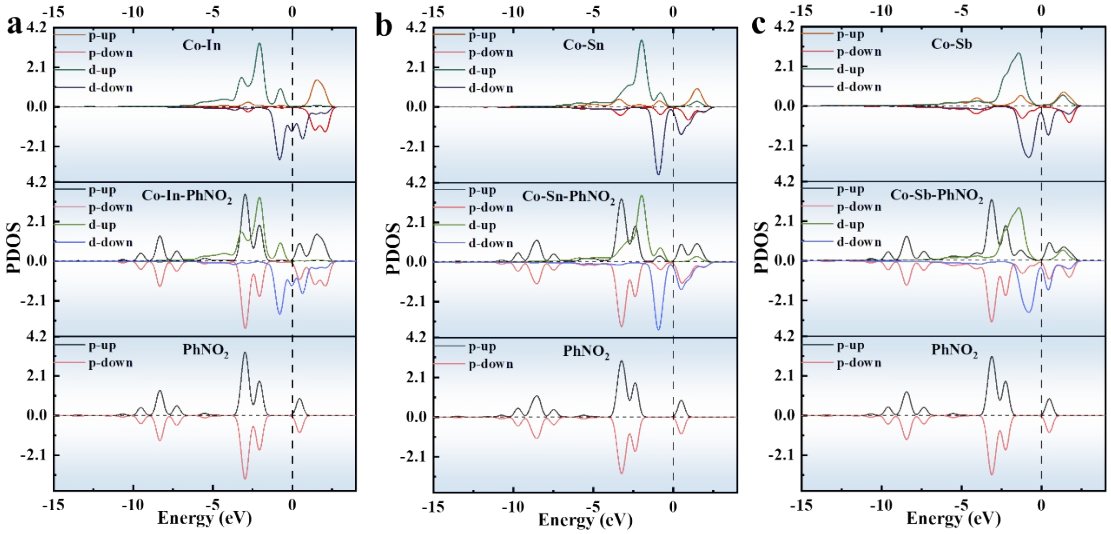

Fig. S18 The PDOS of $PhNO_2$ adsorbed on Co-In-N_6V_4-G, Co-Sn-N_6V_4-G, Co-Sb-N_6V_4-G DACs.

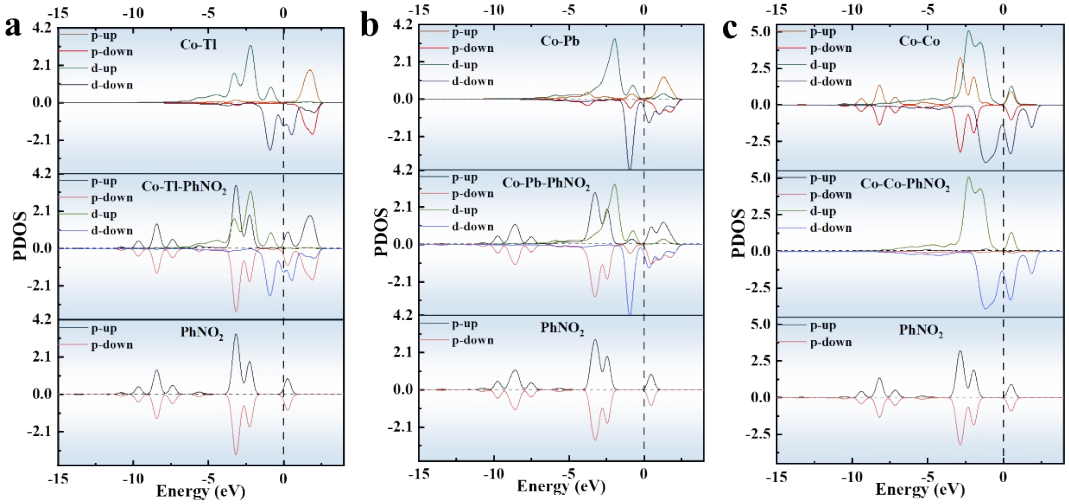

Fig. S19 The PDOS of $PhNO_2$ adsorbed on Co-Tl-N_6V_4-G, Co-Pb-N_6V_4-G, Co-Co-N_6V_4-G DACs.

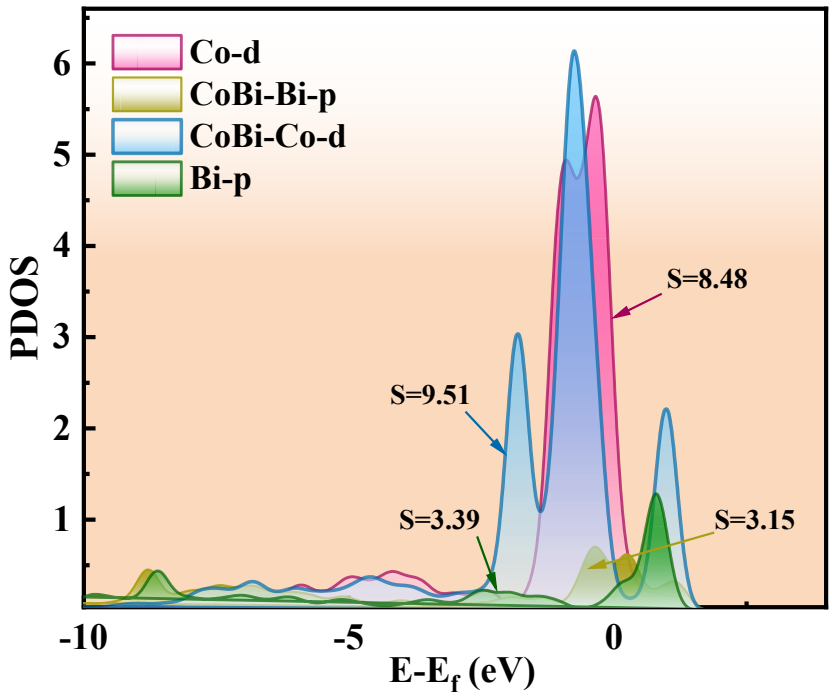

Fig. S20 PDOS analysis of Co-Bi DAC and Co, Bi SACs.

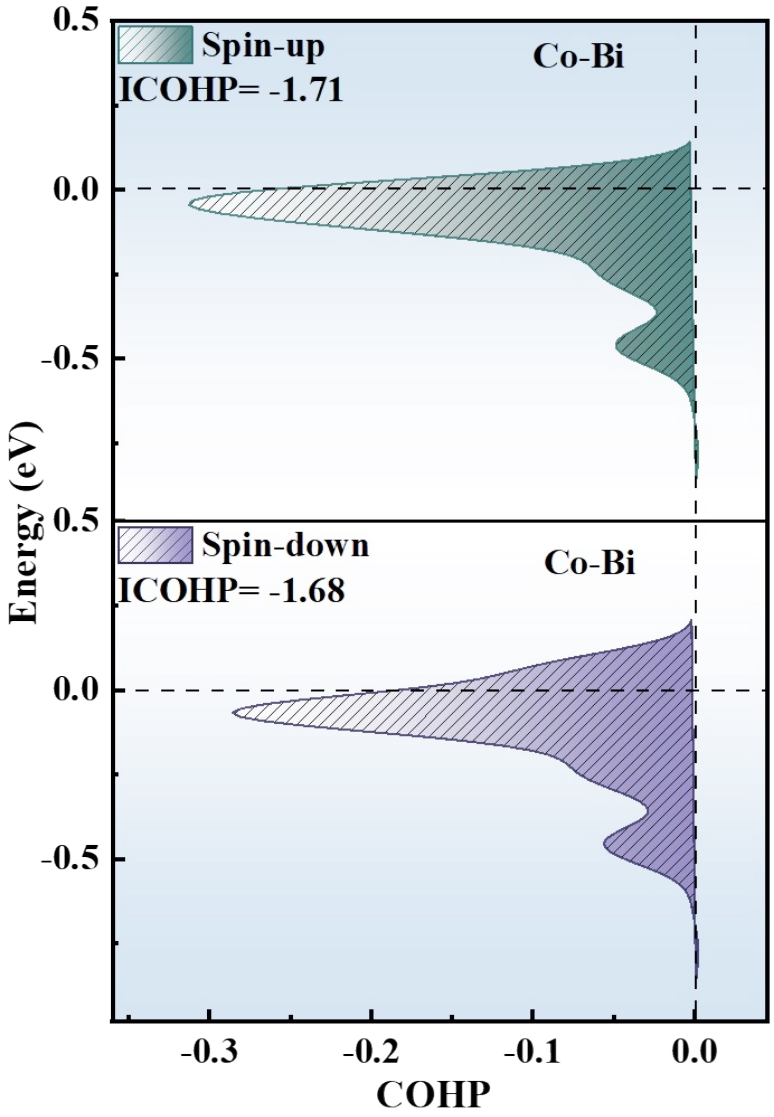

Fig. S21 COHP of Co−Bi bond.

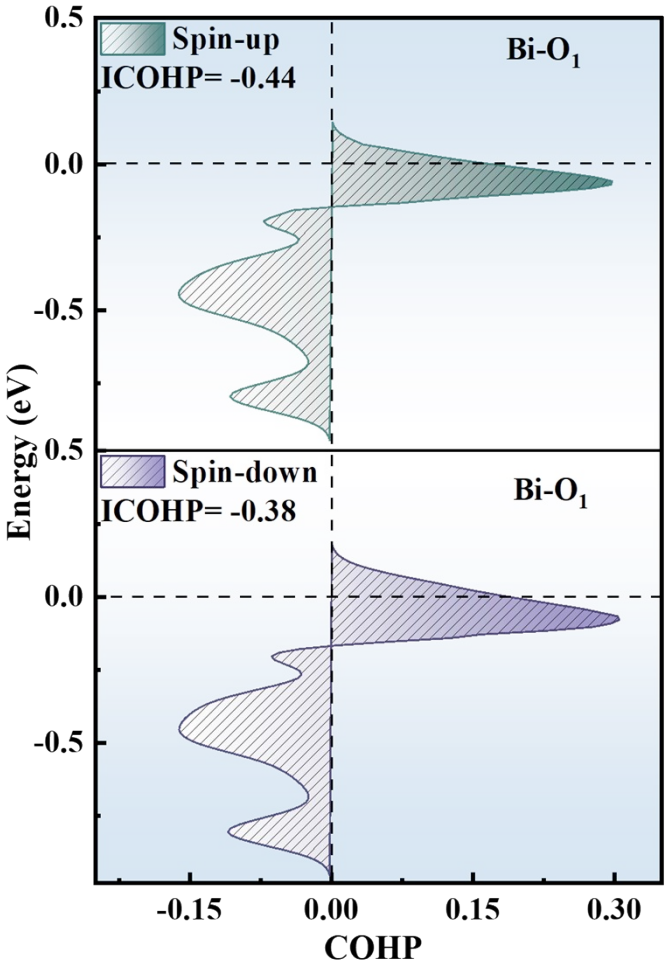

Fig. S22 COHP of Bi−O_1 bond.

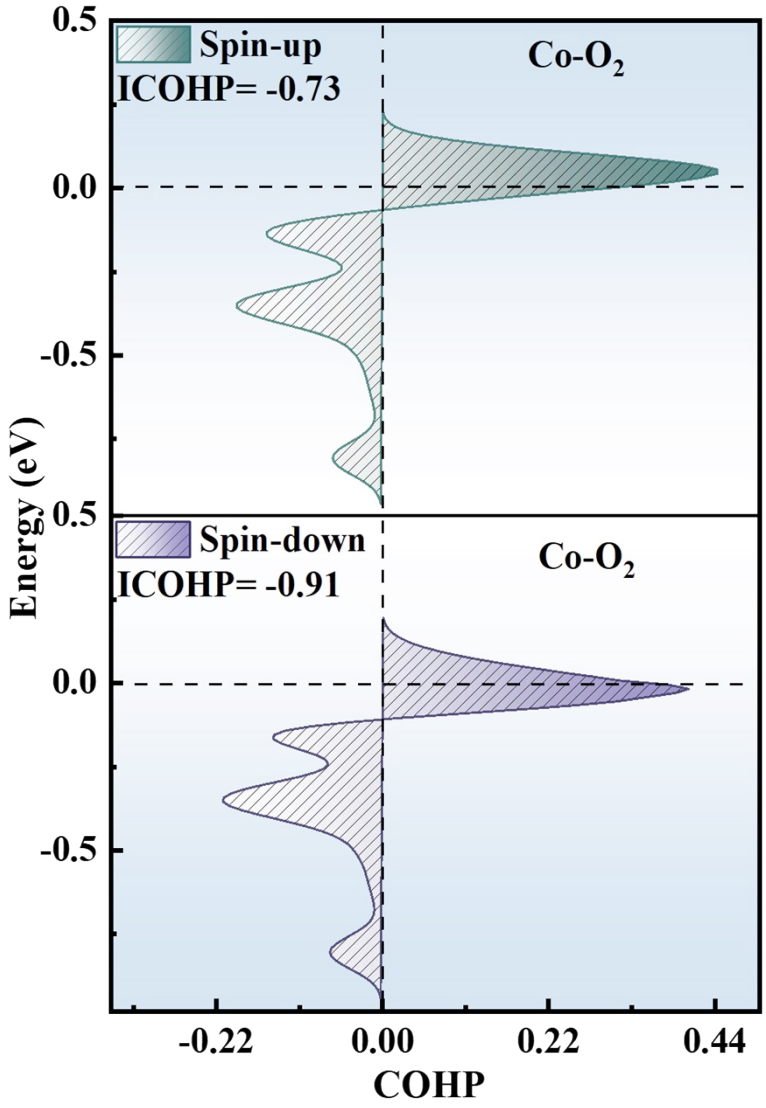

Fig. S23 COHP of Co−O_2 bond.

[1] Y. Duan, Y. Xia, Y. Ling, S. Zhou, X. Liu, Y. Lan, X. Yin, Y. Yang, X. Yan, M. Liang, S. Hong, L. Zhang, L. Wang, Regulating Second-Shell Coordination in Cobalt Single-Atom Catalysts toward Highly Selective Hydrogenation, ACS Nano, 18 (2024) 21326-21335.